JUSAN SCIENCE

Journal of Engineering and Environmental Systems

ISSN (Print): 3135-2510; ISSN (Online): 3135-2529

journal homepage: https://jusanscience.com/journals/jees

Research Article

Development of a Hybrid Material: Superhydrophobic Nanoparticles in Paraffin Matrices for Water-Repellent Applications

Mergen Zhazitov[1*], Beksultan Akilbekov[1], Muhammad Abdullah[1]

[1]Renewable Energy Laboratory, National Laboratory Astana (NLA), Nazarbayev University, Kabanbay Batyr 53, Astana 010000, Kazakhstan

Corresponding author: Mergen Zhazitov mergen.zhazitov@nu.edu.kz

https://doi.org/10.66973/jees.26.004

Article info:

Received: 08 February 2026 / Revised: 04 April 2026 / Accepted: 15 April 2026 / Published: 16 April 2026

Zhazitov, M., Abdullah, M., & Akilbekov, B. (2026). Development of a Hybrid Material: Superhydrophobic Nanoparticles in Paraffin Matrices for Water-Repellent Applications. *Journal of Engineering and Environmental Systems*, 1, 42-56. https://doi.org/10.66973/jees.26.004

Abstract: In this article, we report on the fabrication and characterization of superhydrophobic materials based on zinc oxide (ZnO) nanoparticles embedded in a paraffin matrix. The aim is to create an effective and simple method for designing superhydrophobic materials with improved water repellency through the synergistic effect of surface roughness and low surface energy. The ZnO nanoparticles in paraffin solution were uniformly dispersed through sonication. The solution was then evaporated to obtain the superhydrophobic material. The superhydrophobicity of the material was characterized by scanning electron microscopy (SEM), X-ray diffraction (XRD), Raman spectroscopy, and contact angle measurements. The superhydrophobicity of the material is confirmed by achieving contact angles greater than 150°. The results were attributed to the hierarchical surface feature and hydrophobicity. The structural properties confirmed the presence of ZnO in its crystalline form and uniform distribution in the paraffin matrix. In addition, density functional theory (DFT) calculations were performed to confirm the superhydrophobicity. The results revealed weak interactions between paraffin and ZnO through van der Waals forces. Conversely, strong interactions between water molecules and ZnO were observed, thus confirming superhydrophobicity. The findings in this article confirm an effective method for designing superhydrophobic materials with various applications.

Keywords: Superhydrophobic materials; Zinc oxide nanoparticles; Paraffin matrix; Surface wettability; Contact angle; Hierarchical structure; Nanocomposite materials; Density functional theory (DFT).

1 Introduction

Materials with superhydrophobic properties have been widely studied in recent times due to their remarkable water-repellent properties, which have been defined by a water contact angle greater than 150° and a sliding angle less than 10° [1], [2] . Such materials have been widely studied for their potential in mimicking naturally occurring materials, such as the lotus leaf, which exhibits remarkable self-cleaning properties due to the ability of water droplets on its surface to bead up and roll off, thereby

https://doi.org/10.66973/jees.26.004

cleaning the surface in the process [3], [4] . Superhydrophobic materials have also been studied for their vast potential in various industrial and environmental applications, ranging from anti-corrosion materials, self-cleaning materials, and oil/water separation materials [5], [6]. Moreover, their remarkable friction-reducing, non-fouling, and nonbiofilm-forming properties make them more relevant in marine and biomedical applications[7], [8]. Paraffin wax is widely used as a phase change material (PCM) due to its high latent heat of fusion, chemical stability, and favorable thermal storage characteristics [9], [10]. These properties make paraffin suitable for applications such as building energy storage, solar thermal systems, and temperature regulation in electronic devices [11], [12]. However, its inherently low thermal conductivity significantly limits its efficiency in systems requiring rapid heat transfer, thereby necessitating material modification strategies[13], [14] . To address this limitation, recent studies have focused on developing composite materials by incorporating nanoparticles into paraffin matrices. In particular, the integration of superhydrophobic nanoparticles has emerged as a promising approach to simultaneously enhance thermal conductivity and introduce water-repellent functionality [15], [16]. This hybridization strategy enables the retention of paraffin's thermal storage capabilities while improving its surface and interfacial properties[17], [18]. Furthermore, nanoparticle incorporation has been shown to enhance the mechanical stability, durability, and long-term performance of paraffin-based systems [19]. The present study aims to synthesize and characterize paraffin-based composites containing superhydrophobic nanoparticles and to evaluate their wettability and thermal energy storage performance. Emphasis is placed on commonly used nanoparticles such as silica (SiO_2) and titanium dioxide (TiO_2), which are effective in creating hierarchical surface roughness and promoting hydrophobic behavior [20]. By systematically analyzing nanoparticle–matrix interactions, this work seeks to contribute to the design of advanced multifunctional materials for improved thermal management and environmental sustainability.

2 Experimental part

2.1 Materials

Zinc oxide nanoparticles (ZnO NPs) with diameters of less than 200 nm were provided by LLP "LabPharm" (JHD™). Zinc oxide (molar mass: 81.39 g/mol) is a white powder with a density of approximately 5.606 g/cm³ at 20°C and is insoluble in water. Paraffin wax was purchased from a local supermarket, specifically candle-grade paraffin from the brand Love 2Art, conforming to GOST 23683-89. Paraffin wax is a hydrophobic material commonly used in water-repellent applications due to its low surface energy and melting point of approximately 50–60°C. All materials were used as received without further purification.

2.2 Surface Modification and Water Contact Angle Measurements

For wettability analysis, the ZnO–paraffin hybrid material was deposited onto clean glass substrates (microscope slides) using a drop-casting method. Prior to coating, the glass substrates were ultrasonically cleaned in ethanol and deionized water for 10 minutes each and dried under ambient conditions. The prepared ZnO–paraffin dispersion was applied onto the substrate and allowed to dry at room temperature for 48 hours to ensure complete solvent evaporation and formation of a uniform coating layer. Water contact angle (WCA) measurements were performed using a Dataphysics OCA 15 Pro goniometer. A droplet of deionized water with a volume of 5 μL was gently placed onto the sample surface using a microsyringe. For each sample, measurements were conducted at five different locations to account for surface heterogeneity, and the reported values represent the average ± standard deviation. All measurements were carried out at room temperature under ambient laboratory conditions.

2.3 Fabrication of ZnO hydrophobic nanoparticles

One gram of paraffin was dissolved in 15 milliliters of hexane and stirred at 75°C for 15–20 minutes to ensure complete dissolution. Subsequently, 0.5 grams of zinc oxide (ZnO) nanoparticles were introduced into the paraffin solution, and the mixture was subjected to sonication for 10 minutes to ensure uniform dispersion of the nanoparticles. Following sonication, the mixture was stirred at ambient temperature for an additional 15 minutes. The rotation speed during both stirring phases is a critical parameter; based on our experiments, a speed in the range of 180–360 rpm was found to yield optimal

https://doi.org/10.66973/jees.26.004

results. After preparation, the mixture was dried for 2 days to remove any residual solvent before further processing. To avoid the potential negative effects of hexane usage, d-limonene can be used as a non-toxic alternative solvent. It is an environmentally friendly, biodegradable, and effective solvent for paraffin dissolution. ZnO hydrophobic nanoparticles preparation method was illustrated in Figure 1.

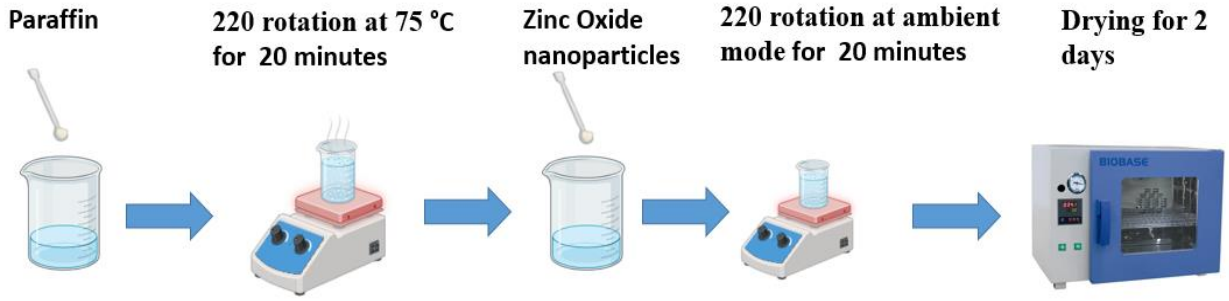

Figure 1. Preparation of ZnO nanoparticles dispersed in paraffin solution, illustrating the process of nanoparticle dispersion and solvent evaporation steps.

2.4 Characterization Techniques

The surface hydrophobicity of the prepared hybrid material was evaluated by measuring water contact angles (WCA) using a goniometer (Dataphysics OCA 15 Pro, Filderstadt, Germany). Scanning electron microscopy (SEM) (Zeiss Auriga Crossbeam 540, Carl Zeiss, Oberkochen, Germany) was used to examine the morphology of the hybrid material in its dried form. X-ray diffraction (XRD) and Raman spectroscopy were employed to analyze the structural and chemical characteristics of the composite. XRD analysis was conducted using system equipped Bragg-Brentano and parallel-beam optics with high-speed 2D detector. λ=1.5046 Cu radiation source was utilized, with scans performed over 2θ° of 10-80° and at 5 min^{-1} rate. These analyses confirmed the uniform dispersion of ZnO nanoparticles within the paraffin matrix and the effectiveness of the resulting material in achieving water-repellent properties.

In this study, Density Functional Theory (DFT) was employed to investigate the structural and electronic properties of representative paraffin segments and their interactions with ZnO and water molecule. The model systems (Figure 2) were carefully designed to reflect realistic configurations, guided by earlier experimental and computational findings [21], [22], [23], [24] . Three main systems were considered: (i) pure paraffin chains, (ii) paraffin in the presence of ZnO, and (iii) paraffin in the presence of ZnO and explicit water molecule. This comparative framework enabled systematic analysis of the influence of ZnO incorporation in the presence and absence of water on molecular geometry, stability, and noncovalent interactions.

2.5 DFT calculations

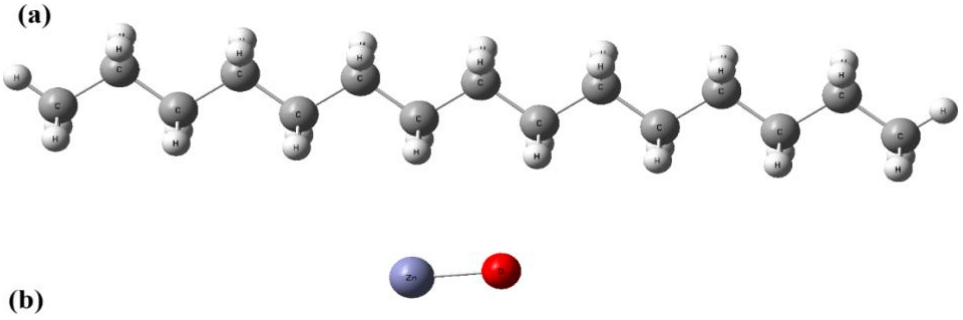

https://doi.org/10.66973/jees.26.004

Figure 2. 3D structures of (a) paraffin, and (b) ZnO.

All DFT calculations were carried out using the GAUSSIAN16 software package [25], [26]. The B3LYP functional combined with the LANL2DZ basis set [27], [28] and Grimme's D3(BJ) dispersion correction was adopted to capture van der Waals interactions, which play a key role in paraffin–ZnO binding. Geometry optimizations were performed with tight convergence criteria, and the optimized structures were confirmed as true minima through vibrational frequency analyses. Post-processing analyses were performed using GaussView [26], Multiwfn [29], and VMD [30]. The following properties were extracted: (i) optimized molecular geometries, (ii) molecular electrostatic potential (MEP) maps, (iii) visualization of noncovalent interactions (NCI), (iv) reduced density gradient (RDG) isosurfaces, and (v) critical point characterization within the framework of Quantum Theory of Atoms in Molecules (QTAIM).

3 Results and Discussion

3.1 Scanning Electron Microscopy (SEM) Analysis

The SEM images (Figure 3) provide detailed information regarding the morphology, particle distribution, and surface architecture of the developed hybrid material composed of superhydrophobic nanoparticles embedded within paraffin matrices for water-repellent applications. These morphological characteristics are critically important because both nanoscale roughness and low surface energy directly influence the hydrophobic and anti-wetting performance of the coating. At lower magnifications, shown in Figures 3(a) and 3(b), the surface exhibits relatively uniform coverage with densely distributed nanoparticles throughout the paraffin matrix, indicating successful formation of the hybrid composite material. The absence of severe agglomeration or phase separation suggests good compatibility between the inorganic nanoparticles and the hydrophobic paraffin phase, resulting in a stable and homogeneous coating structure. Such uniform dispersion is essential for ensuring consistent water-repellent behavior across the coated surface.

At higher magnifications, illustrated in Figures 3(c) and 3(d), the nanoscale morphology of the particles becomes clearly visible. The nanoparticles exhibit irregular polyhedral, semi-spherical, and rod-like morphologies with particle sizes ranging approximately from 93 nm to 206 nm. These nanosized structures significantly enhance the surface roughness of the hybrid material, which is one of the primary requirements for achieving superhydrophobicity according to the Cassie–Baxter wetting model. The hierarchical micro/nanostructured surface promotes the entrapment of air pockets beneath water droplets, thereby reducing the effective liquid–solid contact area and increasing water repellency. Consequently, the rough surface morphology observed in the SEM images is highly favorable for obtaining high water contact angles and low droplet adhesion.

The paraffin matrix plays an equally important role in the hybrid system due to its intrinsically low surface energy and hydrophobic nature. Within the developed material, the nanoparticles mainly contribute nanoscale texturing and structural roughness, whereas paraffin acts as the hydrophobic binding medium that lowers the surface free energy of the coating. The synergistic interaction between surface chemistry and hierarchical roughness is therefore responsible for the enhanced water-repellent properties of the hybrid material. In addition, the SEM images indicate that the nanoparticles are effectively anchored within the paraffin matrix without excessive aggregation, which may contribute to improved coating durability and long-term stability during practical applications.

Furthermore, the interconnected arrangement of nanoparticles observed at higher magnifications may provide additional resistance against water penetration by forming a compact protective surface layer. Similar morphological features have been widely reported in superhydrophobic hybrid

https://doi.org/10.66973/jees.26.004

coatings, where nanoscale particles combined with hydrophobic organic matrices generate surfaces with excellent anti-wetting and self-cleaning performance. The SEM analysis confirms the successful fabrication of a hierarchically rough hybrid material with well-dispersed superhydrophobic nanoparticles embedded in paraffin matrices, demonstrating structural characteristics highly suitable for advanced water-repellent applications.

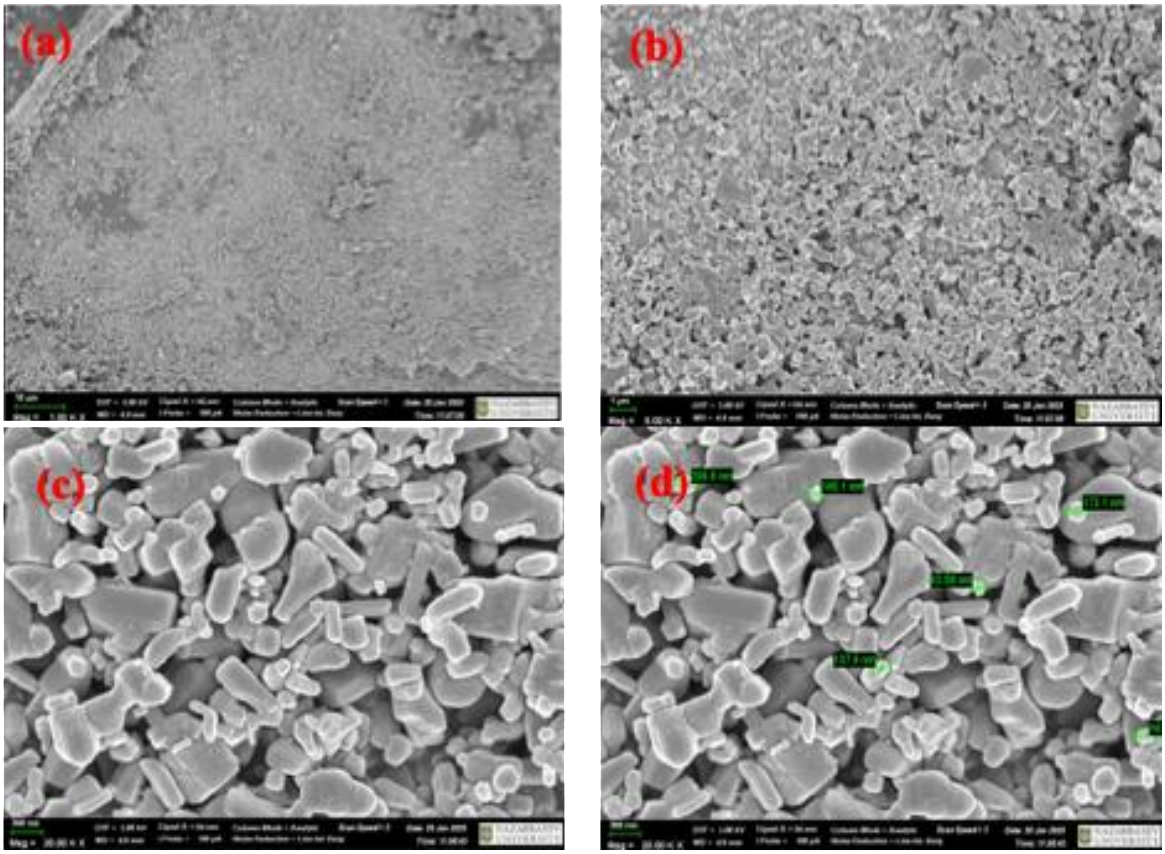

Figure 3. SEM images of the hybrid material at different magnifications: (a) 10 μm, (b) 1 μm, (c) 300 nm, and (d) 300 nm with particle size measurements.

3.2 XRD Results

The X-ray diffraction (XRD) pattern of ZnO incorporated with paraffin, as shown in Figure 4, confirms the crystalline nature of the synthesized material. The diffraction peaks at 2θ values of approximately 31.8°, 34.4°, 36.3°, 47.5°, 56.6°, 62.8°, and 67.9° correspond to the (100), (002), (101), (102), (110), (103), and (112) planes of the hexagonal wurtzite ZnO structure, respectively, as per the JCPDS #36-1451 database. These peaks indicate that the ZnO phase is well-crystallized. The strong intensity of the (002) peak suggests a preferential orientation along the c-axis, which is often associated with nanostructured ZnO, such as rods or platelets. The absence of additional peaks confirms the phase purity of the ZnO. The broad baseline in the XRD pattern may be attributed to the amorphous nature of paraffin, which does not exhibit any sharp diffraction peaks. Overall, the XRD analysis highlights that the incorporation of paraffin does not disrupt the crystallinity or phase integrity of ZnO.

https://doi.org/10.66973/jees.26.004

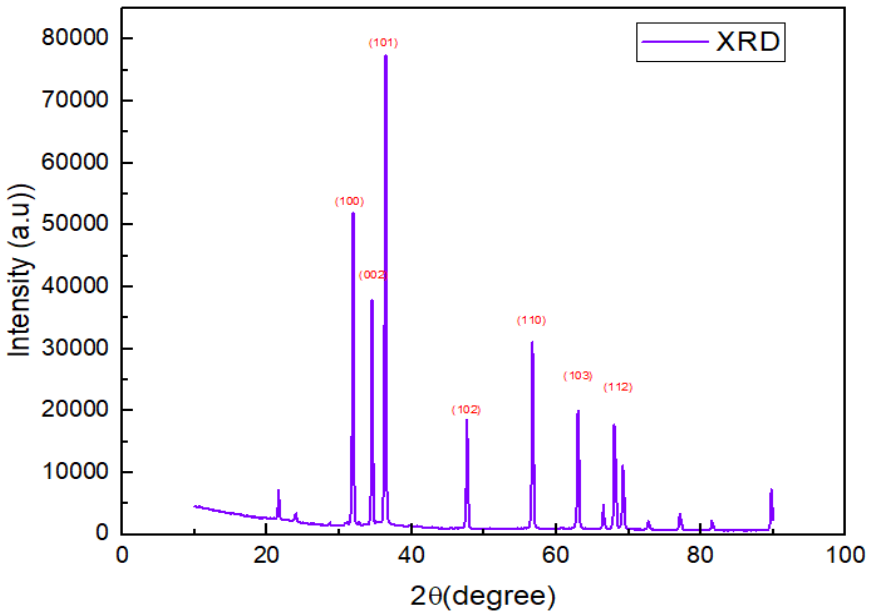

Figure 4. X-ray diffraction (XRD) pattern of ZnO with paraffin. The sharp diffraction peaks correspond to the hexagonal wurtzite structure of ZnO, while the broad baseline reflects the amorphous contribution from paraffin.

3.3 Raman Spectroscopy Analysis

Raman spectroscopy was employed to analyze the structural and chemical composition of the ZnO modified with paraffin (Figure 5). The spectrum exhibits characteristic vibrational modes of ZnO, including a prominent E2 (high) peak around 437 cm^{-1}, associated with the wurtzite phase of ZnO, confirming its crystalline structure. Additionally, the A1(LO) and E1_11(LO) modes observed near 570–583 cm^{-1} suggest the presence of oxygen vacancies or structural defects within the ZnO lattice. The intense peaks in the range of 2800–3000 cm^{-1} correspond to the C-H stretching vibrations of paraffin, confirming its successful modification onto the ZnO surface. Furthermore, minor peaks between 1000 and 1500 cm^{-1} are attributed to C-H bending and C-C skeletal vibrations from paraffin, further supporting the presence of organic functional groups. The combination of these Raman signatures validates the structural integrity of ZnO while confirming the incorporation of paraffin onto its surface.

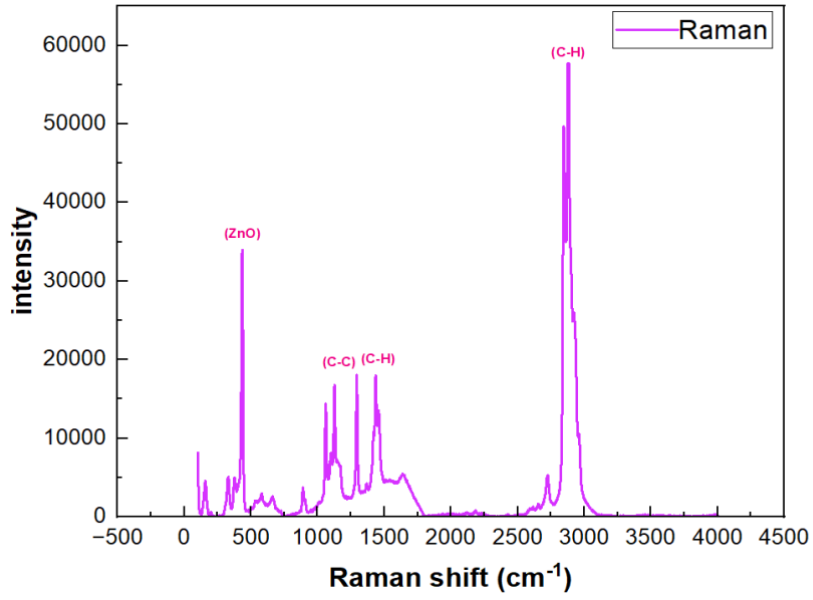

https://doi.org/10.66973/jees.26.004

Figure 5. Raman spectra of fabricated modified paraffin.

3.4 Hydrophobic and Superhydrophobic Behavior

Superhydrophobic nanoparticles modified with paraffin demonstrate excellent water-repellent properties, as evidenced by their water contact angles of 153° and 149° (Figure 6). These values are a clear indicator of successful surface modification, as superhydrophobic materials are typically characterized by contact angles greater than 150°, signifying their ability to repel water effectively. The paraffin coating introduces a low-energy hydrophobic layer, while the nanoscale roughness of the particles enhances the effect by creating a hierarchical structure that traps air at the interface. This combination reduces the contact area between water and the solid surface, forcing water droplets to form nearly spherical shapes that easily roll off. The measured contact angles confirm that the modification process effectively transformed the nanoparticles into superhydrophobic materials, achieving the desired surface properties.

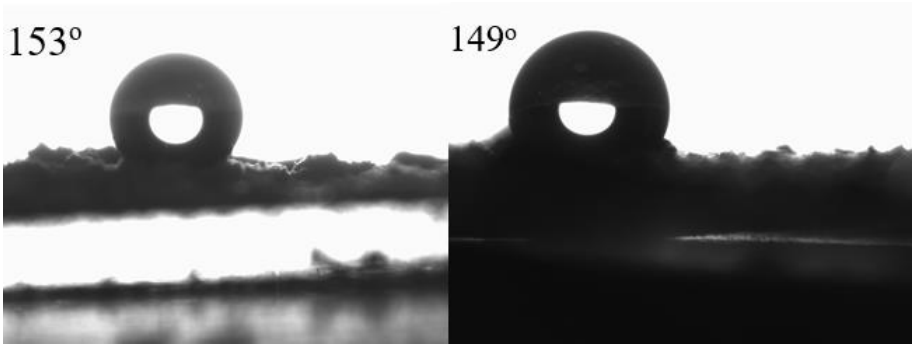

Figure 6. Contact angle measurements.

3.5 DFT results

Optimized structures

Figure 7 shows optimized molecular structures of paraffin chains under different conditions, as investigated using Density Functional Theory (DFT). The first structure, (a), depicts a pure paraffin chain, which has adopted a stable, extended zigzag conformation characteristic of an alkane in its lowest energy state. This linear arrangement is a result of the staggered conformation of C-C single bonds, minimizing steric hindrance between hydrogen atoms. The second structure, (b), introduces a zinc oxide (ZnO) molecule to the system. The ZnO molecule is observed to interact with the paraffin chain, but the interaction appears to be a non-covalent interaction, likely due to van der Waals forces. The ZnO molecule appears to be situated near the middle of the chain, where it can maximize its van der Waals interactions with multiple CH_2 groups.

https://doi.org/10.66973/jees.26.004

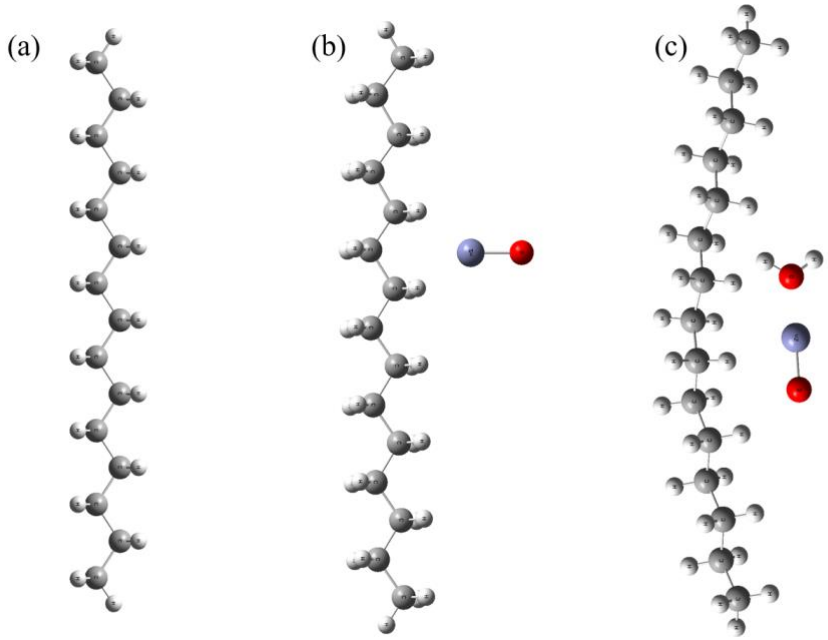

Figure 7. Optimized structures of (i) paraffin, (ii) paraffin with ZnO, and (iii) paraffin with ZnO in the presence of water molecule.

Finally, structure (c) shows the system with both ZnO and an explicit water molecule. The most significant change here is the clear interaction between the ZnO and the water molecule, forming a coordinated complex. The water molecule, being highly polar, likely forms a strong interaction with the ZnO, possibly a Lewis acid-base interaction where the oxygen of water donates an electron pair to the zinc atom. This strong interaction with water appears to influence the ZnO's position relative to the paraffin chain. The paraffin chain itself remains largely unchanged structurally, but the presence of the water-ZnO complex may alter the overall stability and non-covalent interaction landscape of the entire system. This highlights the crucial role of water in mediating the interaction between inorganic compounds like ZnO and organic molecules like paraffin.

Molecular electrostatic potential maps

Based on the provided Figure 8 of the molecular electrostatic potential (MEP) maps, a clear analysis of the electronic properties of the three systems can be conducted.

In Figure 8(a), the MEP map for the pure paraffin chain shows a relatively uniform, weak electrostatic potential across the molecule. The color gradient, ranging from red (negative potential) to blue (positive potential), is very subtle. The paraffin chain is composed of nonpolar C-C and weakly polar C-H bonds, resulting in an essentially neutral surface. The slight variations in potential are due to minor, localized electron density fluctuations, but overall, the map confirms the nonpolar nature of the paraffin molecule.

Figure 8(b) introduces the ZnO molecule, and a dramatic change in the MEP map is observed. The paraffin chain retains its nonpolar characteristic, with a mostly green-blue potential. However, the ZnO molecule displays a strong dipole, and interactions in paraffin become less important. Presence of ZnO forces nearby carbon and hydrogen atoms to exhibit higher charges compared to other atoms in the chain.

Finally, in Figure 8(c), the introduction of a water molecule further modifies the electrostatic landscape. The water molecule, being highly polar, orients itself to interact with the ZnO. Their interactions result in less polar interactions in the paraffin chain, which

https://doi.org/10.66973/jees.26.004

was present in paraffin with ZnO. This is a possible explanation of the hydrophobic nature of fabricated material.

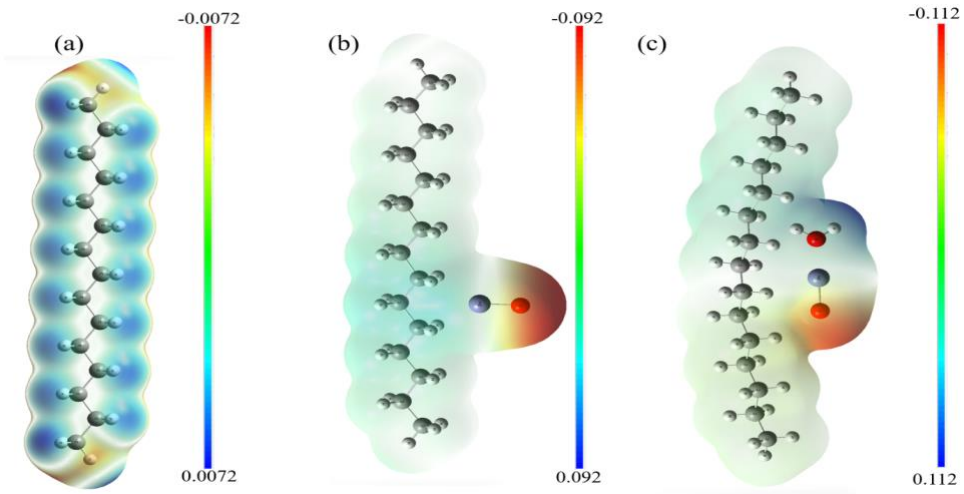

Figure 8. Molecular electrostatic potential maps of (i) paraffin, (ii) paraffin with ZnO, and (iii) paraffin with ZnO in the presence of water molecule.

Visualization of noncovalent interactions

Based on the provided noncovalent interaction (NCI) plots, we can discuss the nature of the interactions within the three molecular systems.

In Figure 9(a), the NCI plot for the pure paraffin chain shows no significant noncovalent interactions. The plot is essentially blank, confirming the absence of strong attractions or repulsions within the molecule. This is expected, as the molecule consists of saturated C-C and C-H bonds, with interactions primarily governed by the covalent bonds holding the structure together. The lack of any NCI isosurfaces (the colored regions) indicates that there are no significant non-bonding interactions like hydrogen bonds or strong van der Waals forces within the chain itself.

https://doi.org/10.66973/jees.26.004

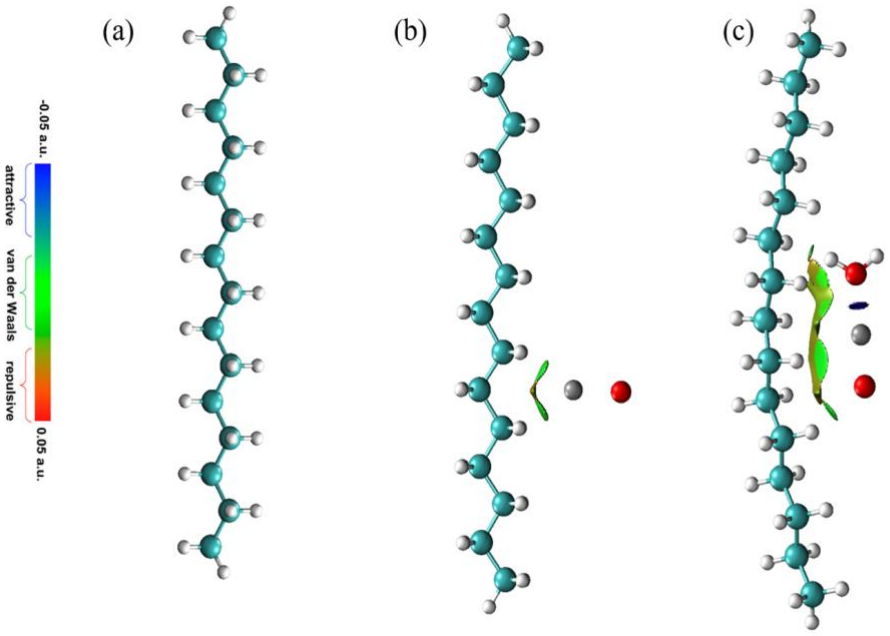

Figure 9. Noncovalent interactions of (a) paraffin, (b) paraffin with ZnO, and (c) paraffin with ZnO in the presence of water molecule.

Figure 9(b) introduces the ZnO molecule, and the NCI plot reveals a weak attractive van der Waals interaction between the paraffin chain and the ZnO molecule. This is represented by a small, faint green isosurface between the ZnO molecule and the paraffin chain. This green color indicates a weak attraction, consistent with the non-polar nature of the paraffin chain and the polar, yet non-covalently bound, ZnO.

In Figure 9(c), the presence of the water molecule dramatically changes the noncovalent interaction landscape. The plot now shows two distinct regions of interaction. A prominent blue isosurface appears between the water molecule and the ZnO molecule signifying a strong attractive interaction, likely a hydrogen bond between the hydrogen atom of the water molecule and the oxygen atom of the ZnO. Simultaneously, a green, van der Waals interaction region still exists between the paraffin chain and the ZnO-water complex, similar to the interaction observed in Figure 8(b). This indicates that the paraffin chain is still weakly interacting with the polar complex through van der Waals forces. The NCI analysis thus confirms weak interactions between water and paraffin, providing possible explanations for hydrophobic nature of the material.

Reduced density gradient (RDG) isosurfaces

Based on the provided Reduced Density Gradient (RDG) plots, we can analyze the types and strengths of noncovalent interactions within the three molecular systems. The color scale indicates the nature of the interaction: blue represents strong attractive interactions (like hydrogen bonds), green indicates weak van der Waals interactions, and red signifies strong repulsive (steric) interactions. The x-axis, sign(λ2)ρ, is a key indicator, with negative values corresponding to attractive interactions and positive values to repulsive ones.

In Figure 10(a), the RDG plot for the pure paraffin chain shows a single large peak centered around a value close to zero on the x-axis, with the color predominantly green. This indicates that the molecule is held together by weak, noncovalent van der Waals forces acting between the CH_2 and CH_3 groups. There are no significant peaks in the negative (attractive) or positive (repulsive) regions, confirming the absence of strong hydrogen bonds or

https://doi.org/10.66973/jees.26.004

steric clashes. This plot is characteristic of a simple, nonpolar alkane.

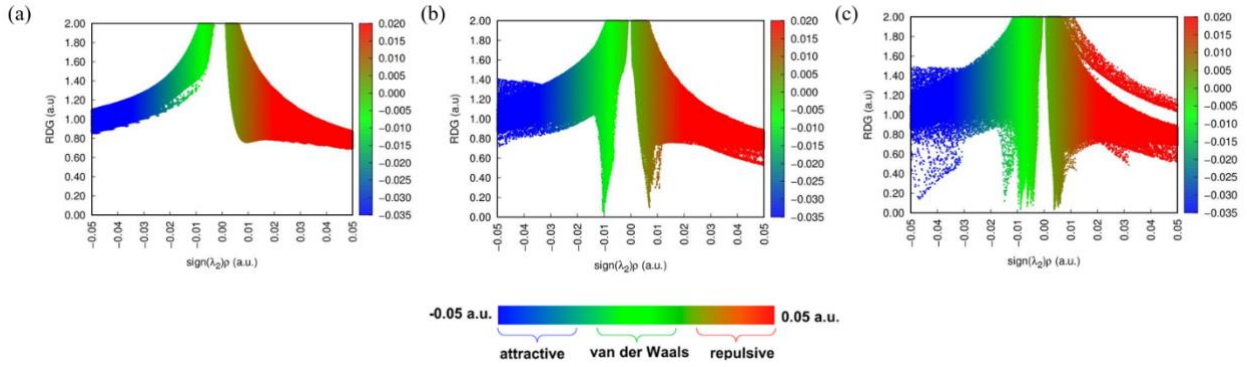

Figure 10. Reduced density gradients of (i) paraffin, (ii) paraffin with ZnO, and (iii) paraffin with ZnO in the presence of water molecule.

Figure 10(b) shows the RDG plot for the paraffin chain with the ZnO molecule. The plot is very similar to the pure paraffin plot, with a large green peak representing the van der Waals forces within the paraffin chain itself. Additionally, a new, small green peak appears in the low-density, low-sign(λ2)ρ region. This new peak corresponds to the weak van der Waals attraction between the paraffin chain and the ZnO molecule. The lack of any significant blue or red peaks indicates that the interaction is neither a strong hydrogen bond nor a significant steric repulsion.

Figure 10(c) illustrates the most complex system, with the paraffin chain, ZnO, and a water molecule. The plot now features a distinct peak in the blue region of the x-axis (negative values), indicating a strong attractive interaction. This corresponds to the hydrogen bond formed between the water molecule and the ZnO. A small red peak is also visible at positive x-values, which may represent minor steric clashes within the more crowded complex. Results of RDG complements previous findings and supports our qualitative claims.

Critical point characterization

The critical points analysis, often derived from Quantum Theory of Atoms in Molecules (QTAIM), provides insights into the bonding and noncovalent interactions within a molecular system.

In Figure 11(a), representing the pure paraffin chain, the absence of any bond critical points (BCPs) between non-bonded atoms is notable. The only critical points present would be those corresponding to the C-C and C-H covalent bonds, which are not explicitly highlighted as inter-atomic BCPs in the context of noncovalent interactions.

Figure 11(b), depicting paraffin with ZnO, reveals the presence of several bond critical points (small orange spheres) between the paraffin chain and the ZnO molecule. These BCPs are indicative of weak noncovalent interactions, specifically van der Waals attractions. The interaction paths, visualized as lines connecting the atoms through these BCPs, show that the ZnO molecule is interacting with multiple CH_2 groups along the paraffin chain. The presence of these BCPs, even if weak, provides topological evidence for the attractive forces previously suggested by the NCI and RDG analyses.

https://doi.org/10.66973/jees.26.004

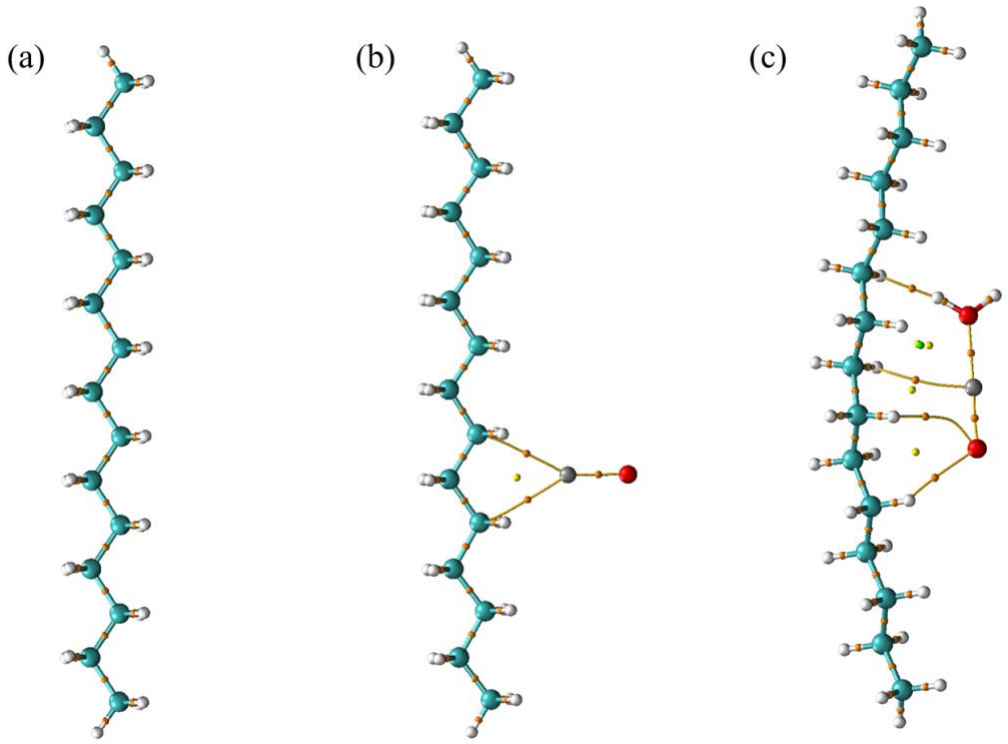

Figure 11. Critical points of (i) paraffin, (ii) paraffin with ZnO, and (iii) paraffin with ZnO in the presence of water molecule.

Finally, Figure 11(c), for paraffin with ZnO and a water molecule, shows a more complex and informative set of critical points. A very prominent bond critical point (colored green) is observed directly between the oxygen atom of the water molecule and the zinc atom of ZnO, and possibly another between a hydrogen of water and the oxygen of ZnO. These BCPs indicate strong attractive interactions, consistent with the formation of a hydrogen bond between water and ZnO. This strong interaction leads to a significant rearrangement of critical points around the ZnO-water complex compared to Figure 11(b). Furthermore, several weaker BCPs (orange spheres) are still present between the paraffin chain and the newly formed ZnO-water complex, signifying the continued presence of van der Waals interactions. This visual confirms the previous observations from NCI and RDG plots: there are no significant noncovalent interactions within the isolated paraffin chain itself, beyond the inherent van der Waals forces.

4 Conclusion

The study demonstrates the successful fabrication of a paraffin–ZnO hybrid material with strong water-repellent performance. Incorporating ZnO nanoparticles into the paraffin matrix and dispersing them through sonication produced a uniform micro/nanostructured surface, which is essential for achieving superhydrophobicity. Experimental measurements showed water contact angles above 150°, confirming the formation of a superhydrophobic coating. Microscopy and structural analyses verified that ZnO maintained its crystalline integrity while being well distributed within the paraffin. The rough topology created by the nanoparticles, combined with the intrinsically low surface energy of paraffin, generated the hierarchical interface required to minimize water–solid contact. Theoretical calculations supported the experimental observations at the molecular level. DFT, MEP, NCI, RDG, and QTAIM analyses consistently indicated that paraffin interacts only weakly with ZnO through van der Waals forces, while water preferentially forms strong interactions

with ZnO. This explains why the paraffin layer can effectively shield the surface and maintain repellency. Although the coating performs reliably within moderate temperatures, paraffin's softening at higher temperatures and brittleness at very low temperatures may limit extreme-environment durability. Future improvements could involve stabilizers or alternative hydrophobic modifiers to widen the operational range. Overall, the hybrid approach provides a simple, scalable pathway toward multifunctional materials suitable for self-cleaning, anti-corrosion, and separation technologies, while also offering molecular-scale insight for further optimization.

Funding
This research received no external funding.

Author Contributions
B.A.: Methodology, Software, Writing – Original Draft. M.A.: Methodology, Investigation, Resources. M.Z.: Supervision, Conceptualization, Writing – Review & Editing.

Ethics Approval and Consent to Participate
This study did not involve human participants or animals. Therefore, ethical approval and informed consent were not required.

Data Availability Statement
The data supporting the findings of this study are available from the corresponding author upon reasonable request.

Supporting Information
Not applicable.

Conflict of Interest
The authors declare no conflict of interest.

AI Use Disclosure
No AI tools were used to generate scientific results, data, figures, or interpretations. All analyses, conclusions, and scientific content were developed by the authors.

References

[1] M. R. Mujawar, R. B. Sawant, D. A. Kumbhar, A. M. Sargar, and S. R. Kulal, "A review on superhydrophobic surfaces: Fundamentals, fabrications and applications," *Int. J. Multidiscip. Res.*, vol. 9, p. 56, 2023.

[2] H. Zhang, Y. Liu, Z. Zhang, M. Hua, and G. Dong, "A superhydrophobic surface patterned with hydrophilic channels for directional sliding control and manipulation of droplets," *Surf. Coat. Technol.*, vol. 409, Art. no. 126836, 2021, https://doi.org/10.1016/j.surfcoat.2021.126836.

[3] M. S. Hasan and M. Nosonovsky, "Lotus effect and friction: Does nonsticky mean slippery?," *Biomimetics*, vol. 5, Art. no. 28, 2020,. https://doi.org/10.3390/biomimetics5020028

[4] R. Dalapati, S. Nandi, C. Gogoi, A. Shome, and S. Biswas, "Metal–organic framework (MOF) derived recyclable, superhydrophobic composite of cotton fabrics for the facile removal of oil spills," *ACS Appl. Mater. Interfaces*, vol. 13, pp. 8563–8573, 2021, https://doi.org/10.1021/acsami.0c21337

[5] H. Y. Erbil, "Practical applications of superhydrophobic materials and coatings: Problems and perspectives," *Langmuir*, vol. 36, pp. 2493–2509, 2020, https://doi.org/10.1021/acs.langmuir.9b03908

[6] S. Aziz, T. Talha, A. R. Mazhar, J. Ali, and D. W. Jung, "A review of solar-coupled phase change materials in

buildings," *Materials*, vol. 16, Art. no. 5979, 2023, https://doi.org/10.3390/ma16175979

[7] C. Hu, S. Liu, B. Li, H. Yang, C. Fan, and W. Cui, "Micro-/nanometer rough structure of a superhydrophobic biodegradable coating by electrospraying for initial anti-bioadhesion," *Adv. Healthc. Mater.*, vol. 2, pp. 1314–1321, 2013. https://doi.org/10.1002/adhm.201300021

[8] F. Meng, C. Che, Y. Wu, J. Wei, J. Rong, X. Yang, *et al*., "Thermal storage performance of a shell and tube phase change heat storage unit with different thermophysical parameters of the phase change material," *Processes*, vol. 12, Art. no. 123, 2024, https://doi.org/10.3390/pr12010123

[9] G. Hailu, "Seasonal solar thermal energy storage," in *Thermal Energy Battery with Nano-Enhanced PCM*, M. Sheikholeslami Kandelousi, Ed. London, U.K.: IntechOpen, 2019, ch. 2, pp. 11–31, doi: 10.5772/intechopen.79576.

[10] Y. Li, L. Li, and J. Sun, "Bioinspired self-healing superhydrophobic coatings," *Angew. Chem.*, vol. 122, pp. 6265–6269, 2010,https://doi.org/10.1002/ange.201001258

[11] I. Yilgor, S. Bilgin, M. Isik, and E. Yilgor, "Tunable wetting of polymer surfaces," *Langmuir*, vol. 28, pp. 14808–14814, 2012, https://doi.org/10.1021/la303180k

[12] R. S. Almufarij and M. E. Mohamed, "Green synthesis of a carbon quantum dots-based superhydrophobic membrane for efficient oil/water separation," *Materials*, vol. 16, Art. no. 5456, 2023, https://doi.org/10.3390/ma16155456

[13] L. Fan, B. Li, Q. Wang, A. Wang, and J. Zhang, "Superhydrophobic gated polyorganosilanes/halloysite nanocontainers for sustained drug release," *Adv. Mater. Interfaces*, vol. 1, Art. no. 1300136, 2014, https://doi.org/10.1002/admi.201300136

[14] X. Wang and S. C. Jana, "Tailoring of morphology and surface properties of syndiotactic polystyrene aerogels," *Langmuir*, vol. 29, pp. 5589–5598, 2013. https://doi.org/10.1021/la400492m

[15] S. Pang, F. Liu, Y. Zhang, Z. Dong, Q. Su, W. Wang, *et al*., "Construction of functional superhydrophobic biochars as hydrogen transfer catalysts for dehydrogenation of N-heterocycles," *ACS Sustain. Chem. Eng.*, vol. 9, pp. 9062–9077, 2021, https://doi.org/10.1021/acssuschemeng.1c02322

[16] S. T. Yohe, J. D. Freedman, E. J. Falde, Y. L. Colson, and M. W. Grinstaff, "A mechanistic study of wetting superhydrophobic porous 3D meshes," *Adv. Funct. Mater.*, vol. 23, pp. 3628–3637, 2013. https://doi.org/10.1002/adfm.201203111

[17] S. Yang, J. Lin, Z. Zhang, C. Zhang, X. Zheng, W. Xie, *et al*., "Advanced engineering materials for enhancing thermal management and thermal safety of lithium-ion batteries: A review," *Front. Energy Res.*, vol. 10, Art. no. 949760, 2022. https://doi.org/10.3389/fenrg.2022.949760.

[18] Y. Wang and X. Gong, "Superhydrophobic coatings with periodic ring structured patterns for self-cleaning and oil–water separation," *Adv. Mater. Interfaces*, vol. 4, Art. no. 1700190, 2017. https://doi.org/10.1002/admi.201700190

[19] A. Beagan, J. Lin, Y. Lu, M.E. Mohamed, Sustainable and efficient oil-water separation using bio tin oxide-based superhydrophobic membrane, Front. Water 6 (2024) 1390739. https://doi.org/10.3389/frwa.2024.1390739

[20] N. Kydyrbay, M. Zhazitov, M. Abdullah, T. Duisebayev, Y. Tezekbay, A. Aldongarov, M. Karibayev, N. Nuraje, O. Toktarbaiuly, Structural, surface, and theoretical investigation of hydrophobic-modified nanodiamond

powders, Sci. Rep. 15 (2025) 24329. https://doi.org/10.1038/s41598-025-10027-9.

[21] J.C. Stockert, B. López-Arias, P. Del Castillo, A. Romero, A. Blázquez-Castro, Replacing xylene with n-heptane for paraffin embedding, Biotech. & Histochem. 87 (2012) 464–467. https://doi.org/10.3109/10520295.2012.701764

[22] D. C. Perera and J. C. Rasaiah, "Exchange functionals and basis sets for density functional theory studies of water splitting on selected ZnO nanocluster catalysts," *ACS Omega*, vol. 7, 2022.12556–12569. https://doi.org/10.1021/acsomega.1c05666

[23] B. Myrzakhmetov, M. Karibayev, Y. Wang, and A. Mentbayeva, "Density functional theory investigation of intermolecular interactions for hydrogen-bonded deep eutectic solvents," *Eurasian Chem. J.*, vol. 26, pp. 29–36, 2024. https://doi.org/10.18321/ectj1563.

[24] B. Myrzakhmetov, A. Akhmetova, A. Bissenbay, M. Karibayev, X. Pan, Y. Wang, *et al*., "Chitosan-based biopolymers for anion-exchange membrane fuel cell application," *R. Soc. Open Sci.*, vol. 10, Art. no. 230843, 2023. https://doi.org/10.1098/rsos.230843

[25] M. J. Frisch, G. W. Trucks, H. B. Schlegel, G. E. Scuseria, M. A. Robb, J. R. Cheeseman, *et al*., *Gaussian 16, Revision C.01*. Wallingford, CT, USA: Gaussian, Inc., 2016.

[26] R. D. Dennington, T. A. Keith, and J. M. Millam, *GaussView, Version 6*. Shawnee Mission, KS, USA: Semichem Inc., 2016.

[27] P. M. W. Gill, B. G. Johnson, J. A. Pople, and M. J. Frisch, "The performance of the Becke–Lee–Yang–Parr (B–LYP) density functional theory with various basis sets," *Chem. Phys. Lett.*, vol. 197, pp. 499–505, 1992.https://doi.org/10.1016/0009-2614(92)85807-M.

[28] C. E. Check, T. O. Faust, J. M. Bailey, B. J. Wright, T. M. Gilbert, and L. S. Sunderlin, "Addition of polarization and diffuse functions to the LANL2DZ basis set for p-block elements," *J. Phys. Chem. A*, vol. 105, pp. 8111–8116, 2001.https://doi.org/10.1021/jp011945l.

[29] T. Lu and F. Chen, "Multiwfn: A multifunctional wavefunction analyzer," *J. Comput. Chem.*, vol. 33, pp. 580–592, 2012. https://doi.org/10.1002/jcc.22885.

[30] W. Humphrey, A. Dalke, and K. Schulten, "VMD: Visual molecular dynamics," *J. Mol. Graph.*, vol. 14, pp. 33–38, 1996. https://doi.org/10.1016/0263-7855(96)00018-5.